VARIATION WITH TEMPERATURE IN PHOTOPYROELECTRIC SPECTROSCOPY AND ELECTRICAL PARAMETERS OF ZnO + 1.0 MnO_2 + 0.8 Co_3O_4 + xBi_2O_3 + yTiO_2 CERAMICS

N. NASIR[a], M. KASHIF[b], N. SABIR[b], Z. RIZWAN[a,*]
[a]*Department of Applied Sciences, Faculty of Science National Textile University, Sheikhupur Road, Faisalabad, Pakistan*
[b]*Department of Physics, G.C University, Faisalabad, Pakistan*

Band gap energy (E_g) of doped ZnO ceramic with 1MnO, 0.8 Co_3O_4, xBi_2O_3 + yTiO_2 where x = y = 0.6, 1 mol%. Different sintering times 1-4 hours have been studied in 300 to 800 nm wavelength range using a technique Photopyroelectric spectroscopy (PPES). The Graph is plotted between $(\rho h\upsilon)^2$ and $h\upsilon$. E_g is assessed from the plot which is about 2.03, 2.07 eV for the samples sintered for 2 hours at low and high doping levels, respectively. The increase in steepness factor (σ_A, in A-region and σ_B, in B-region) is related to sintering time at low and high doping level. Barrier height (ϕ_B) is 0.96, 0.89 eV for lower and higher doping level at 4 hour sintering time, respectively. The dielectric constant varied with the increases of sintering time. The dissipation factor Tanδ is decreased with the increase of sintering time. The X-ray diffractometry analysis shows that the crystal structure of ZnO doped with different MnO mol% remains to be of hexagonal type at all sintering times. Furthermore, it was observed that few feeble peaks are found related to the new phase Bi_2MnTiO_4, Zn_2TiO_4, $MnTi_4O_4$ and $Bi_4Ti_3O_{12}$ at higher sintering time at both doping levels. The grain size ranges increased with the increase of sintering time and relative density decreased. Sintering time of the sample increases the density is decreased from (90.6, 88. to 88, 86 %) at lower and higher doping levels, respectively.

(Received September 14, 2018; Accepted January 16, 2019)

Keywords: Photopyroelectric spectroscopy, Energy band gap, ZnO, Barrier height

1. Introduction

Semi-conductors ceramic of (ZnO) are extensively used to detect the gas. Even nanoparticles of ZnO is used as a photocatalyst. This use of ZnO for mineralization of toxic inorganic and organic compounds makes ZnO, prominent in applied fields [1]. Doping of such materials is a vital and effective path for increasing optical as well as magnetic properties of semiconductor materials. In particular, doping of transition metals (TM) into the lattice of ZnO enhances its optical absorption. This absorption influence the E_g [2]. The increased applicability of these sensors is piezoelectric transducers solar cells electrodes, transparent conducting films, phosphors, [4] and varistors. ZnO as a varistor possess the energy absorption capability against surges of various types. It is broadly used as a protective device. It has a fast response to overvoltage transients. These sensors can sense surges and clamp such surges in a speed of nano-seconds. It responses constantly without any damage, in thousands of times [3, 4]. Typically varistors are made-up by the sintering of ceramic ZnO with many other metal oxides (MO). MO in small quantities such as MnO, Cr_2O_3, Bi_2O_3, Sb_2O_3, Co_3O_4, Al_2O_3, Y_2O_3 and Pr_6O_{11} etc. To enhance the stability of ZnO varistor and its nonlinear response these additives are proved as the main tool [5]. Current-Voltage characteristics have been studied extensively for ZnO ceramic based varistor [5, 6]. The investigations on optical absorption measurements have been completed. It is important to acquire information on the optical absorption of ZnO ceramic doped with metal oxides. Such investigations are compulsory to understand the electrical behavior of doped ZnO on electronic states of doped ZnO ceramic at different levels. In this study,

*Corresponding author: zahidrizwan64@gmail.com

photopyroelectric spectroscopy of MnO_2, Co_3O_4, Bi_2O_3, and TiO_2 doped ZnO ceramic have been presented at various sintering times.

2. Materials and methods

2.1. Sample preparation

Zinc Oxide of brand Alfa Aesar with purity of 99.9% was doped with 1.0 MnO, 0.8 Co_3O_4, xBi_2O_3, and $yTiO_2$ where x = y = 0.6 and 1 mol%. Ethanol was mixed in 25 g of product at each mol% and stirred for 20 hours. The slurry was cleaned and dried out in the air. Before pre-sintering, the mixture was crushed to make a fine particle powder. The powder was pre-sintered at temperatures 700 °C at 4°C $min^{-1}$of each mol% and divided into three parts. To attain a sufficient strength all these samples were crushed and polyvinyl alcohol (PVA 0.8 wt %) was added as a binder. To avoid cracks, PVA binder was added in the last pressed sample. The fine powder was pressed with a force of 2000 kg/cm^2 using a Specac press. The lubricant, zinc stearate was used to make disks of 01 cm in diameter with a thickness of 0.1 cm. Pellets were sintered at a sintering temperature of 1270 °C for 1-4 hours with a one-hour interval. The samples were air-annealed at the heating rate of 6°C min^{-1}. Then all samples at room temperature were cooled down at the cooling rate of 6°C per minute. The density of the samples was determined by the geometrical method. One disk was crushed for 90 minutes. The powder was sieved using a mesh screen (75micron) for XRD analysis and PPES.

2.2. Photopyroelectric measurements

To study material's optical properties, a non-radiative tool, PPE spectroscopy from photothermal science have been used [7]. The photothermal effect is the main phenomenon of this technique. The measurement of variations in temperature due to light-induced periodic heating in the sample can be done using the pyroelectric (PE) transducer film. Nonradiative de-excitation processes [16], the absorption of light takes place within the solid sample. The temperature fluctuates, as a result of the heat diffusion to the adjacent PE film. As a result of the temperature changes a PE voltage, at a frequency (ω) of modulation, is produced. This PE voltage in PE film is given by the equation [8]:

$$V(\omega)\, pI_d\, \Delta T / \varepsilon = < \Delta T >$$

The parameters used in the equation are

p =PE coefficient.

I_d = thickness of film.

ε = dielectric constant of film.

$< \Delta T >$ = rise in average temperature of the film.

Optical excitation wavelengths ranging from 300 to 800 nm signal amplitude was recorded using a complete system of PPE spectrometer as described elsewhere [9] that is known as PPE spectrum which can be called an excitation spectrum. Powder from each sample was again crushed in the deionized water for PPE measurement. Few drops of each combination were fallen on an Al metal foil having an area about 1.6 cm^2. Aluminum foils were dried out in the air to prepare a thin solid layer of the fine powder. Aluminum foil was positioned in contact using conductive grease to PPE film transducer [10]. Light source "Xenon arc lamp 1 kW (Oriel 6921)" was used in a spectrophotometer. At the (9 Hz) frequency light beam was mechanically chopped. PPE spectrum data of the samples were gathered at room temperature. To gain the actual sample spectrum data was normalized with carbon black PPE spectrum data. The fundamental absorption edge of ZnO is as a result of the direct allowed transition. With excitation light energy (hυ), the optical absorption coefficient (β) fluctuates. It is specified by the following equation [11, 12]:

$$(\beta h\upsilon)^2 = C\,(h\upsilon - E_g)$$

The parameters are as follows:

C = constant independent of photon energy hυ.

E_g =Direct allowed energy band-gap.
ρ =PPE signal intensity.

The signal is directly proportionate to β, So $(\rho h\upsilon)^2$ is related to hυ linearly. From the graph of $(\rho h\upsilon)^2$ against hυ, by extrapolating the linear fitted regions with $(\rho h\upsilon)^2 = 0$ E_g is found.

2.3. Dielectric dispersion measurements

The samples for (100 to 1MHz) frequency dependency of the dielectric constant of doped ceramic ZnO for sintering times (1- 4) hours were scanned at room temperature [13]. For this purpose, the impedance analyzer (Hewlett Packard Model 4192A) was used.

2.4. Microstructure examination

The both of the samples surfaces were ground with SiC paper. To make like a mirror surface diamond suspension (1 μm) were used to polish the surfaces. All polished samples were thermally etched at the temperature 155°C below the sintering temperature for 10 minutes. The surface microstructure was examined of the samples using SEM. The average grain size (d) of the samples was found using the linear intercept method. The crystalline phases of the samples were analyzed using XRD (with CuKα radiation), PANAalytical (Philips) X'Pert Pro PW1830. For the identification of the crystalline phases, X-ray diffraction data were analyzed with the help of X'Pert High Score software.

3. Results and discussion

The main phase observed in the XRD analysis for 0.6 mol% combination of TiO_2 and Bi_2O_3 in the ceramic is ZnO with some other secondary phases. Small peaks of the Bi_2O_3 (ref. code00-018-0244) was detected for 1 and 2 hour sintering time. Few peaks of the secondary phase Bi_2MnTiO_4 (ref. code 00-051-0674) for 3 hours, Zn_2TiO_4 (ref. code 01-073-0578) and $MnTi_4O_4$ (ref. code 01-073-0580) for 4 hour sintering time were detected. When additives Bi_2O_3 and TiO_2 increased to 1 mol%, the secondary phase developed in the ceramic are about the same as developed with the lower additive combination.

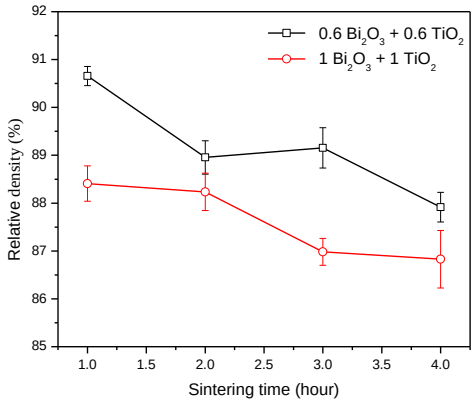

Fig. 1. Variation of density with sintering time.

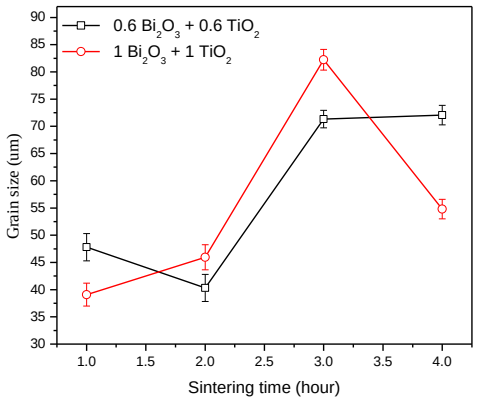

Fig. 2. Variation of grain size with sintering time.

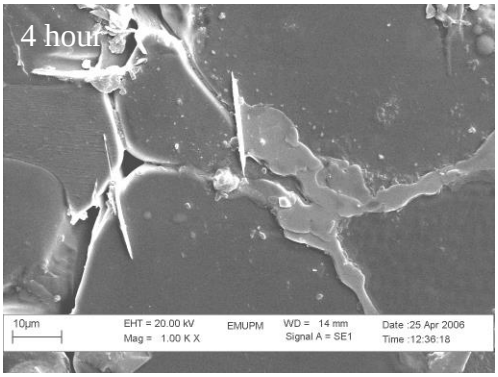

Fig. 3. SEM micrograph for 1 TiO_2 + 1 Bi_2O_3 at 4 h sintering time.

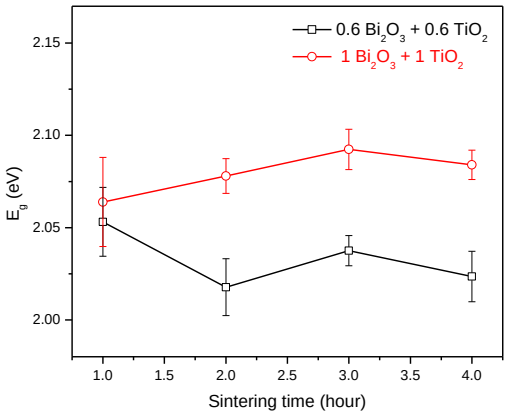

Fig. 4. Variation of E_g with sintering time.

The Bi_2O_3 is detected in the ceramic at 1 and 2 hour sintering time. The secondary phases Zn_2TiO_4 (ref. code 01-073-0578), $Bi_4Ti_3O_{12}$ (01-072-1019) are found for 3 hour sintering time. Zn_2TiO_4 (ref. code 01-073-0578), $Bi_{20}TiO_{32}$ (100-002-100) with a small peak are found for 4 hour sintering time. The relative density of the ceramic decreased from 88.4 to 86.8 % as sintering time increases for ceramic $1TiO_2$ + $1Bi_2O_3$ Fig. 1. When the doping level of TiO_2 and Bi_2O_3 is decreased from 1 to 0.6 mol% then the density decreases from 90.6 to 87.9 % with the increase of the sintering time. The grain size of the ceramics increases as sintering time increases, Fig. 2. The grain size increases from 47.8 to 72 µm with the increase of sintering time for 0.6 TiO_2 + 0.6 Bi_2O_3 combinations. Grain enhancer Bi_2O_3, TiO_2, and MnO_2 are present in the ceramic [15]. When the doping level of the TiO_2 and Bi_2O_3 increased from 0.6 mol% to 1 mol% of TiO_2 and Bi_2O_3, the grain size increased to 82.2 µm until sintering time of 3 hours, grain size decreases rapidly with the increase of So interface states increases and E_g decreases as shown in the Fig. 4. The steepness factor σ_B increases, Fig. 6, when the quantity of the additives Bi_2O_3 and TiO_2 increases from 0.6 to 1 mol% of each showing the decrease in the average thermal energy of the atoms which corresponds to the decrease in the interface states and resultantly, the value of E_g increases slightly with the rise of the sintering time [14]. This indicates that the interface states decreases with the increase of sintering temperature. This may be due to the segregation of Bi_2O_3 and the development of the secondary phases at the higher doping level sintering time. This is due to the phase developed at this sintering time which inhibits the grain growth mechanism. It was also observed that the small grains and some abnormal needle-like grains were seen in the micrograph of ceramics at the higher sintering temperature as compared to the low sintering time, Fig. 3. EDX results display that the Bi_2O_3 is gathered at the grain boundaries. Bi_2O_3 was also present at triple point junctions. It was observed that Mn and Co, Ti have appeared on the grain surface. This shows that their substitution is possible in ZnO lattice. Ti, Mn, Co was also found in

the grain boundaries indicating the secondary phases have been developed in ZnO ceramics. These secondary phases are segregated at grain boundaries.

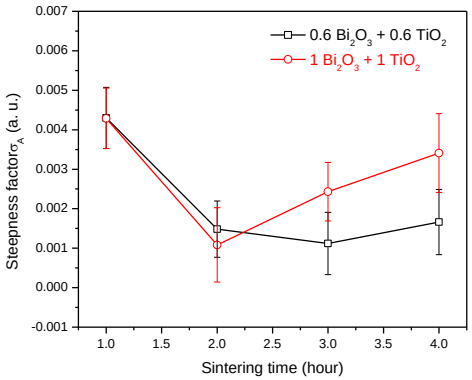

Fig. 5. Effect of sintering time on steepness factor σ_A.

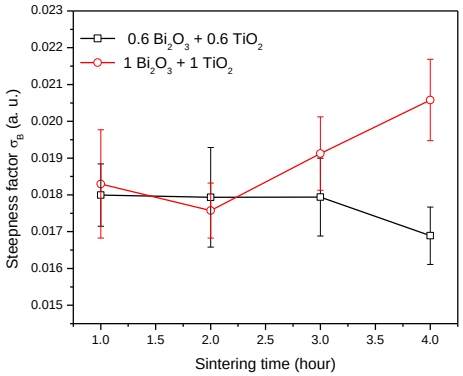

Fig. 6. Effect of sintering time on the steepness factor σ_B.

The value of E_g is decreased from 3.2 eV (pure ZnO) to 2.05 ± 0.02 for the ceramic combination 0.6 Bi_2O_3 + 0.6 TiO_2 for 1 hour sintering time, Fig. 4. This decrease is due to the interface states produced by the combined effect of 0.8 Co_3O_4, 0.6 Bi_2O_3, 0.6 TiO_2, 1 MnO_2. The value of E_g decreased slightly from 2.05 ± 0.02 to 2.02 ± 0.01 eV for this combination of the ceramic with the increase of sintering time. This decrease is very small and is about constant at 2.02 ± 0.01 after 2 hour sintering time. This indicates that the growth of interface states is at saturation limit for the sintering time 2 hour and above. The value of E_g of the ceramic decreases from 3.2 eV (pure ZnO) to 2.06 ± 0.01 when the amount of additive is increased from 0.6 to 1 mol% of Bi_2O_3 and TiO_2 and the combination becomes as ZnO + 0.4 Co_3O_4 + 1 Bi_2O_3 + 1 TiO_2 with the increase of sintering time. This indicates that the E_g value is reduced as a result of the growth of interface states with the higher doping level by the combined effect of 0.8 Co_3O_4, 1 Bi_2O_3, 1 TiO_2, and 1 MnO_2. The value of E_g increases due to the secondary phases developed in the ceramics at the higher temperature. It is also observed that the value of E_g is higher for the higher doping combination.

This increase is about 0.06 ± 0.01 at 2 hour sintering time and above. This may be due to the development of the secondary phases and their segregation at the grain boundaries and at the triple point junctions. The steepness factor σ_A, Fig. 5, decreases with the rise of sintering time with the ceramic combination 0.6 Bi_2O_3+ 0.6 TiO_2 indicates the increase in the PPE signal intensity. This indicates the increase in the structural disordering. So this structural disordering generates the interface states which reduce the value of E_g as shown in Fig. 4 as a result of the growth of interface states and correspondingly, E_g decreases. The steepness factor σ_A increases indicating the decreases in the PPE signal intensity when the amount of additives increases from 0.6 Bi_2O_3+ 0.6 TiO_2 to 1 Bi_2O_3+ 1 TiO_2. This shows that the increase in the structural ordering [16, 17]. The value of σ_A for 1 hour sintering time seems to be an abnormality. This structural ordering is possibly due to the liquid phase Bi_2O_3 and its contribution to making secondary phases and segregates at the particle surfaces and in the grain boundaries. So the interface states decreases and the E_g also increases slightly as shown in Fig. 4. The steepness factor σ_B drops with the increase of sintering time indicating increases in the average thermal energy of the atoms, Fig. 6, for the 0.6Bi_2O_3+ 0.6TiO_2 additives combinations due to the increase in structural disordering [18].

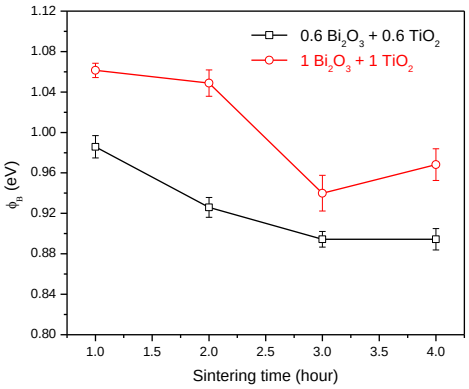

Fig. 7. Variation of barrier height with sintering time.

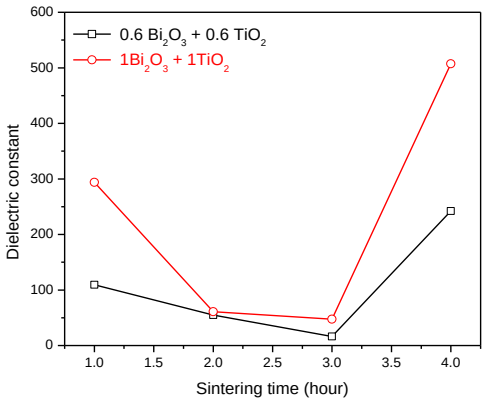

Fig. 8. Variation of dielectric constant with sintering time.

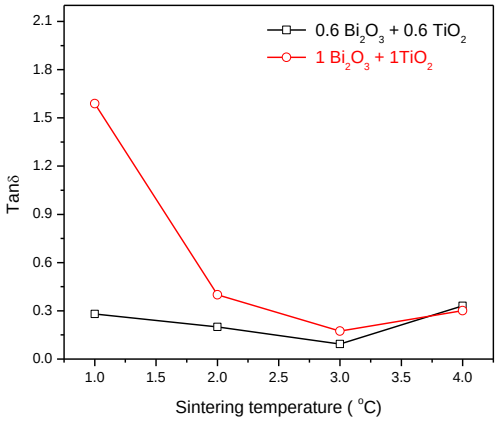

Fig. 9. Variation of dissipation factor with the the increase of sintering temperature

From the current-voltage characteristics, varistor voltage decreases from 695.5 to 619 V/cm for the combination 0.6 Bi_2O_3+ 0.6 TiO_2 with the increase of the sintering time. It is related to the grain size as grain size increases, varistor voltage decreases as the number of grain boundaries decreases. Varistor voltage decreases with the rise of the sintering time and it slightly increases for 4 hour sintering time as grain size decreases for the 4 hour sintering time for the ceramic combination of 1 Bi_2O_3+ 1 TiO_2. The value of nonlinear coefficient (α) decreases with the increase of the sintering time from 14.2 to 7.4 with the increase of the sintering time for the ceramic combination of 0.6 Bi_2O_3+ 0.6 TiO_2. When the amount of additives is increased from 0.6 to 1 mol% then the value of the nonlinear coefficient is maximum 10.7 for the sintering time of 2 hours. The barrier height, Fig 7, is decreasing from 0.98 to 0.89 eV with the increase of the sintering time for the ceramic combination 0.6 Bi_2O_3+ 0.6 TiO_2. Its value is also decreasing from 1.06 to 0.96 eV with the increase of the sintering time for the ceramic combination 1 Bi_2O_3+ 1 TiO_2. The value of barrier height is higher with the higher amount of additives at all sintering times. Dielectric constant [19], Fig. 8, at 1 KHz, decreases from 109 to a minimum value 16 with the rise of sintering time up to 3 hour sintering time and then again surges up to a value of 242 for the ceramic combination 0.6 Bi_2O_3+ 0.6 TiO_2. Its value decreases from 293 to a minimum value 47 with the increase of sintering time up to 3 hour sintering time and then again increases up to a value of 507 for the combination 1 Bi_2O_3+ 1 TiO_2 additives. Its value is higher for the higher combination at all sintering time. This can be directly related to the grain size as $\varepsilon_{app.} = \varepsilon_g$ (d/t). It is found that the value of the dissipation factor (Tanδ) decreases while sintering time increases.

This indicates the Joule heating loss by leakage current and friction heating loss by electric dipole rotation is decreasing, Fig. 9.

4. Conclusion

The X-ray diffraction results and sintering time are correlated with the PPES results. These results indicate the development of secondary phases. The PPES of doped ZnO shows the slight variation in the value of E_g and increase in steepness factor indicates the formation of interfacial states and structural ordering with the increase of sintering time. The value of barrier height decreases with the increase of sintering time. The dielectric constant is minimum for the 3 hours sintering hours. Value of dissipation factor decreases while sintering time increases. This indicates the Joule heating loss by leakage current and friction heating loss.

References

[1] O. K. AL-Duaij, Journal of Optoelectronics and Biomedical Materials **10**, 11 (2018).
[2] M. S. Prathap Reddy, P. T. Poojitha, V. K. M. Smitha Rani, M. Kumar, Journal of Ovonic Research **14**, 55 (2018).
[3] Joshy Jose, M. Abdul Khadar, Mater. Sci. Engg. A **304-306**, 810 (2001).
[4] D. C. Look, Mater. Sci. Engg. B **80**, 383 (2001).
[5] K. Eda, Zinc Oxide Varistors, IEEE Elect. Insul. Mag. **5**, 28 (1989).
[6] Choon-Woo Nahm, Byoung-Chil Shin, Mater. Lett. **57**, 1322 (2003).
[7] A. Minamide, M. Shimaguchi, Y. Tokunaga, Jpn. J. Appl. Phys. **37**, 3144 (1998).
[8] D. P. Almond, P. M. Patel, Photothermal Science and Techniques, Chapman and Hall, London, 91 (1996).
[9] A. Mandelis, Chem. Phys. Lett. **108**, 388 (1984).
[10] A. Minamide, Y. Tokunaga, IEEE Ultrasonic Symp. 865 (1998).
[11] A. Gadalla, M. S. Abdel-Sadek, R. Hamood, Chalcogenide Letters **15**(5), 281 (2018).
[12] J. F. Mohammad, Journal of Non-Oxide Glasses **10**, 27 (2018).
[13] T. R. N. Kutty, S. Ezhilvalavan, Mater. Sci. Engg. B **47**, 101 (1997).
[14] A. Kimura, Y. Ohbuchi, T. Kawahara, Y. Okamoto, J. Morimoto, Jpn. J. Appl. Phys. **40**, 3614 (2001).
[15] L. M. Levinson, H. R. Philipp, Am. Ceram. Soc. Bull. **65**, 639 (1986).
[16] F. Urbach, Phys. Rev. **92**, 1324 (1953).
[17] J. D. Dow, D. Redfield, Phys. Rev. B **5**, 594 (1972).
[18] Taro Toyoda, Satoshi Shimamoto, Mater. Sci. Engg. B **54**, 29 (1998).
[19] S. Ezhilvalavan, T. R. N. Kutty, Mater. Chem. Phys. **49**, 258 (1997).